

# LIX: Implicitly Infusing Spatial Geometric Prior Knowledge into Visual Semantic Segmentation for Autonomous Driving

Sicen Guo<sup>ID</sup>, Zhiyuan Wu<sup>ID</sup>, Qijun Chen, *Senior Member, IEEE*,

Ioannis Pitas, *Life Fellow, IEEE*, Rui Fan<sup>ID</sup>, *Senior Member, IEEE*

**Abstract**—Despite the impressive performance achieved by data-fusion networks with duplex encoders for visual semantic segmentation, they become ineffective when spatial geometric data are not available. Implicitly infusing the spatial geometric prior knowledge acquired by a duplex-encoder teacher model into a single-encoder student model is a practical, albeit less explored research avenue. This paper delves into this topic and resorts to knowledge distillation approaches to address this problem. We introduce the Learning to Infuse “X” (LIX) framework, with novel contributions in both logit distillation and feature distillation aspects. We present a mathematical proof that underscores the limitation of using a single fixed weight in decoupled knowledge distillation and introduce a logit-wise dynamic weight controller as a solution to this issue. Furthermore, we develop an adaptively-recalibrated feature distillation algorithm, including two technical novelties: feature recalibration via kernel regression and in-depth feature consistency quantification via centered kernel alignment. Extensive experiments conducted with intermediate-fusion and late-fusion networks across various public datasets provide both quantitative and qualitative evaluations, demonstrating the superior performance of our LIX framework when compared to other state-of-the-art approaches.

**Index Terms**—semantic segmentation, spatial geometric prior knowledge, knowledge distillation.

## I. INTRODUCTION

IN the domain of data-driven autonomous driving perception, a prevailing consensus among researchers asserts that “the increased availability of well-annotated training data is strongly correlated with improved learning performance.” When examining visual semantic segmentation as an illustrative case, the adoption of data-fusion networks, equipped

with duplex encoders to acquire knowledge from both RGB images and spatial geometric information, consistently demonstrate superior performance compared to conventional single-modal networks trained exclusively on RGB data [1]–[4]. This performance improvement is due to their ability to learn heterogeneous features from a multitude of data sources [5]. RGB images primarily capture rich information related to color and texture within scenes, whereas other visual data sources, commonly designated as “X”, e.g. depth/disparity images [6], HHA maps [7], and surface normal maps [2], contain informative spatial geometric information. The fusion of their features allows for a more comprehensive understanding of the driving environment.

However, a significant limitation of data-fusion networks stems from their dependence on the availability of the “X” data, which can pose constraints in scenarios devoid of range sensors. Additionally, when the accuracy of the “X” data falls below expectations, possibly due to issues such as variations in camera-LiDAR calibration, the fusion of these heterogeneous features can potentially lead to a degradation in the overall performance of visual semantic segmentation [1], as quantitatively demonstrated using the Cityscapes dataset [8], which lacks depth ground truth. As a result, the implicit infusion of spatial geometric prior knowledge from a teacher deep neural network (DNN) model (a data-fusion network trained with RGB-X data) to a student DNN model (a single-modal network trained exclusively with RGB data) emerges as an interesting research direction to be explored.

It is reasonable to consider that knowledge distillation (KD) techniques, initially introduced by Hinton *et al.* [9], can be a viable solution to achieve this objective. These techniques generally fall into two main categories: (a) logit distillation (LD) [9]–[11] approaches, which train the student model to replicate the logits of the teacher network, by minimizing the divergence or distance between the probability distributions generated by the teacher and student networks; and (b) feature distillation (FD) approaches [12]–[18] focusing on leveraging the abundant information available in the activations, neurons, and features of the intermediate layers from the teacher DNN to provide guidance and supervision for the student model training.

Nonetheless, directly applying these existing techniques to our specific problem remains challenging due to three considerations: a) one notable challenge emerges primarily due to the absence of spatial geometric information, leading

This research was supported by the National Natural Science Foundation of China under Grant 62233013, the Science and Technology Commission of Shanghai Municipal under Grant 22511104500, and the Fundamental Research Funds for the Central Universities. The research leading to these results has also received partial funding from the European Commission - European Union (under HORIZON EUROPE (HORIZON Research and Innovation Actions) under grant agreement 101093003 (TEMA) HORIZON-CL4-2022-DATA-01-01). Views and opinions expressed are however those of the authors only and do not necessarily reflect those of the European Union - European Commission. Neither the European Commission nor the European Union can be held responsible for them. (*Corresponding author: Rui Fan*)

Sicen Guo, Zhiyuan Wu, Qijun Chen, and Rui Fan are with the Machine Intelligence & Autonomous Systems (MIAS) Group, the College of Electronics & Information Engineering, Shanghai Research Institute for Intelligent Autonomous Systems, the State Key Laboratory of Intelligent Autonomous Systems, and Frontiers Science Center for Intelligent Autonomous Systems, Tongji University, Shanghai 201804, China (e-mail: {guosicen, gwu, qjchen, rfan}@tongji.edu.cn)

Ioannis Pitas is with the Department of Informatics, University of Thessaloniki, 541 24 Thessaloniki, Greece (e-mail: pitas@csd.auth.gr).

to a huge gap that the student model often struggles to bridge in order to learn the multi-source prior knowledge acquired by the teacher model [19], [20]; b) the differences between teacher and student DNN models, including discrepancies in heterogeneous data feature characteristics such as dimensions, magnitudes, distributions, and more, form as a barrier to the effective infusion of spatial geometric prior knowledge [21]; c) comprehensive feature consistency measurement should be emphasized and requires further exploration, as it has a direct impact on the overall performance of feature distillation [12], [14], [15].

This paper introduces Learning to Infuse “X” (LIX) framework (see Fig. 1), designed to implicitly infuse spatial geometric prior knowledge acquired from a duplex-encoder DNN teacher model into a single-encoder student DNN model. We make three major contributions to address the above-mentioned considerations. We begin by revisiting the LD theory based on decoupled knowledge distillation (DKD) [22] and reformulate its loss as a weighted combination of target class LD (TCLD) and non-target class LD (NCLD) losses. By deriving the gradient of the LD loss with respect to the student logit function, we expose the limitations of the DKD algorithm, which relies on a single fixed weight. Consequently, we design a dynamic weight controller (DWC), capable of generating a weight for each logit, thereby improving the overall LD performance. As for FD, we first introduce an adaptive feature recalibration approach based on kernel regression, which aligns the features of the teacher and student DNN models across various dimensions (spatial, channel, magnitude, and distribution). Finally, we resort to the centered kernel alignment (CKA) [23] algorithm based upon Hilbert-Schmidt independence criterion (HSIC) [24] to formulate our novel FD loss, which quantifies the feature consistency between the teacher and student DNN models. These contributions collectively improve the effectiveness of implicitly infusing spatial geometric prior knowledge into visual semantic segmentation for autonomous driving. In a nutshell, our contributions can be summarized as follows:

- We implicitly infuse spatial geometric prior knowledge into visual semantic segmentation, distilling a teacher duplex-encoder (RGB-X) DNN architecture into a student DNN operating only RGB images.
- We present the novel dynamically-weighted LD (DWLD) algorithm, which extends the DKD algorithm, by assigning an appropriate weight to each logit, resulting in greater performance compared to the baseline algorithm.
- We introduce the novel adaptively-recalibrated FD (ARFD) algorithm that performs: a) feature recalibration via kernel regression; and b) feature consistency measurement leveraging HSIC-based CKA.

We have conducted extensive experiments using representative RGB-X semantic segmentation models on multiple public datasets to quantitatively and qualitatively validate the effectiveness of our introduced novelties.

## II. RELATED WORK

### A. RGB-X Semantic Segmentation

According to the data-fusion stage, state-of-the-art (SoTA) RGB-X semantic segmentation approaches can be grouped into three classes: early fusion, intermediate fusion, and late fusion [25]. Early fusion approaches generally combine RGB images and X data at the input level. Such a straightforward yet simplistic data-fusion strategy has limitations in capturing a deep understanding of the environment [25]. In contrast, intermediate fusion approaches [2], [26] typically extract heterogeneous features from RGB images and X data using duplex encoders. These features are subsequently fused within the encoder to fully exploit their inherent characteristics. Late fusion approaches [27]–[29] are similar to intermediate-level methods and use two parallel encoders (one for RGB images and one for X data) to extract heterogeneous features. However, these methods primarily focus on feature fusion within the decoder. In this paper, we utilize two representative networks, namely SNE-RoadSeg [2] (a computationally intensive network performing intermediate feature-fusion) and MFNet [27] (a lightweight network performing late feature-fusion) to comprehensively validate the effectiveness of our proposed LIX framework.

### B. Knowledge Distillation

The concept of KD was first introduced in [9], with the aim of guiding the student DNN model to mimic the distribution characteristics of the soft targets (the logit generated by the teacher model). Unlike the early KD [9] algorithm, a channel-wise KD (CWKD) [11] algorithm was proposed to address dense prediction tasks, such as image segmentation. CWKD normalizes the activations in each channel to create a probability map. Subsequently, the Kullback-Leibler (KL) divergence algorithm [9] is utilized to minimize the discrepancy between these probability maps generated by the teacher and student DNN models. However, in these previous works, the TCLD and NCLD terms are treated as interdependent and coupled terms. The recent DKD research effort [22] suggests that the coupled formulation of KD limits the effectiveness and flexibility of knowledge transfer, and reformulates the classical KD loss into two independent and decoupled terms.

LD methods depend exclusively on the output logits of the last layer and do not incorporate intermediate-level supervision to ensure feature consistency between the teacher and student DNN models. Such feature-level supervision has been demonstrated to be crucial for effective representation learning, particularly within DNN [30]. The first reported effort in FD was FitNet [31], which directly matches the feature activations in the teacher and student DNN models. Attention transfer (AT) [12] resorts to both activation-based and gradient-based spatial attention maps to realize FD. Several subsequent studies, *e.g.*, similarity-preserving KD (SPKD) [16] and variational information distillation (VID) [17], have sought to reduce the dimension of features during FD to accommodate the increasing depth of modern neural networks. In contrast, factor transfer (FT) [13] employs a paraphraser and a translator to transfer the knowledge (known as ‘factors’ in their study) from the teacher to the student. On the other

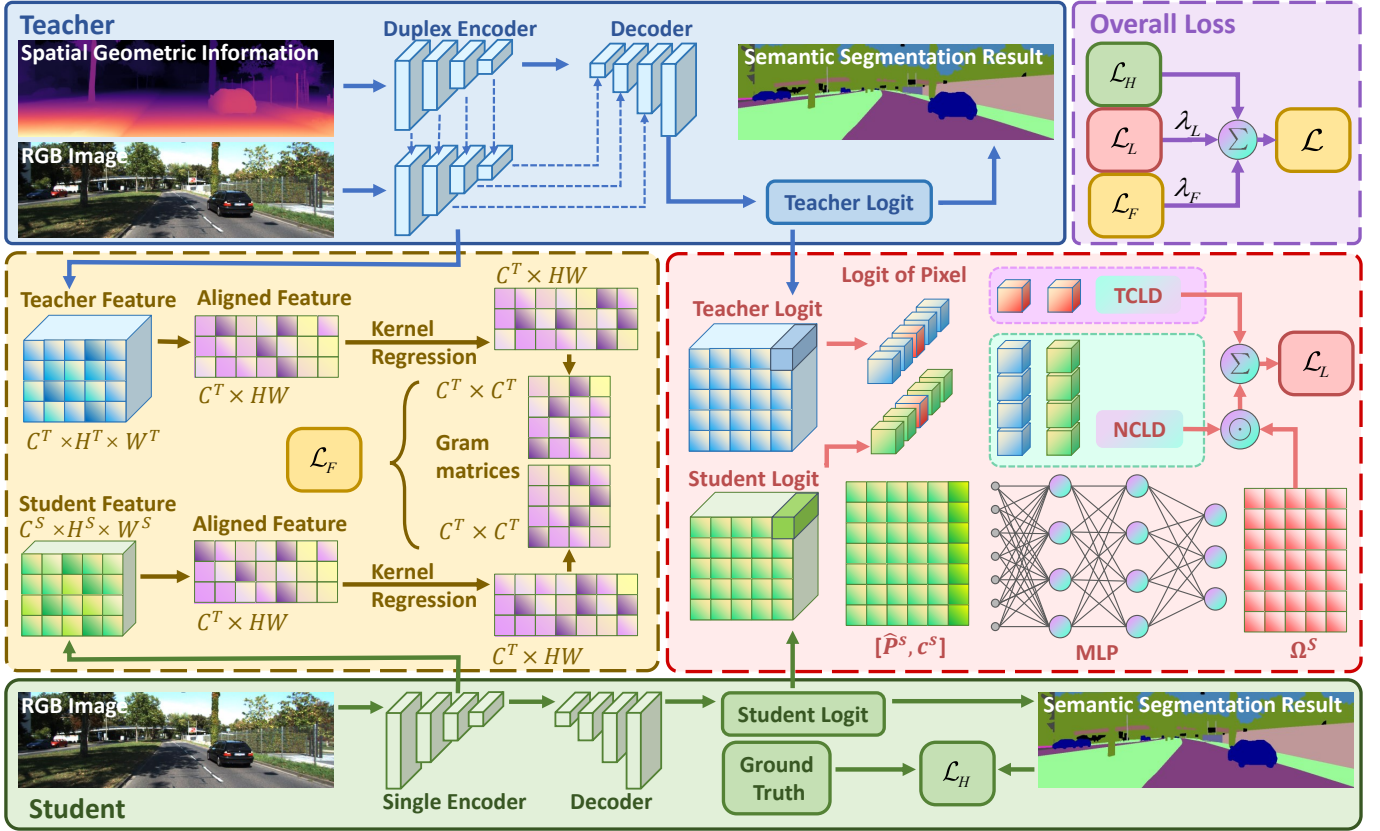


Fig. 1. An overall of our proposed **LIX framework**, which consists of two key components: a) **dynamically-weighted logit distillation** and b) **adaptively-recalibrated feature distillation**.

hand, relational knowledge distillation (RKD) [15] introduces distance-wise and angle-wise distillation losses to penalize structural differences in relations between the teacher and student models. Neuron selectivity transfer (NST) [14] treats KD as a distribution matching problem. It aligns the distributions of neuron selectivity patterns between the teacher and student models by projecting them into a higher dimensional feature space using kernel regression and minimizing the maximum mean discrepancy metric between them.

Neither of the aforementioned algorithms were designed specifically to infuse spatial geometric prior knowledge into semantic segmentation, especially for autonomous driving perception. In this paper, we contribute to both LD and FD. We introduce a logit-wise dynamic weight controller to address the limitations of using a single fixed weight in DKD. Additionally, we develop an adaptively-recalibrated feature distillation algorithm that includes feature recalibration via kernel regression and in-depth feature consistency quantification. Extensive experiments demonstrate the superior performance of our LIX framework compared to all the reviewed algorithms.

### III. METHODOLOGY

#### A. Dynamically-Weighted Logit Distillation

Most past logit distillation methods [9], [11] primarily resorted to more effective regularization and optimization methods, rather than proposing novel distillation strategies. In this subsection, we delve deeper into the LD theory and reframe its loss as the weighted combination of TCLD and

NCLD losses. We derive the gradient of the LD loss with respect to the student logit and expose the limitations of the traditional DKD algorithm [22] that relies on a single fixed weight. Drawing inspiration from these findings, we introduce a novel LD method, which is capable of dynamically generating a weight for each logit, thereby improving the overall performance of spatial geometric prior knowledge infusion.

**Reformulating Logit Distillation.** Let  $\hat{\mathbf{p}} = [\hat{p}_1, \dots, \hat{p}_k, \dots, \hat{p}_C]^\top \in \mathbb{R}^C$  be a column vector, storing the probabilities  $\hat{p}_i = P(y = i | \mathbf{q}) = \exp(z_i) / \sum_{j=1}^C \exp(z_j)$  ( $\forall i \in [1, C] \cap \mathbb{Z}$ ) of pixel  $\mathbf{q}$  belonging to the  $C$  classes, where  $y$  denotes the predicted label of  $\mathbf{q}$  and  $z_i$  denotes its logit with respect to the  $i$ -th class. Let  $\mathbf{b} = [\hat{p}_k, 1 - \hat{p}_k]^\top \in \mathbb{R}^2$  be a binary probability vector of the target class  $k$ . Let  $\hat{\mathbf{p}}_{\setminus k} = \hat{\mathbf{p}} / (1 - \hat{p}_k) = [\hat{p}_{1, \setminus k}, \dots, \hat{p}_{k-1, \setminus k}, \hat{p}_{k+1, \setminus k}, \dots, \hat{p}_{C, \setminus k}]^\top \in \mathbb{R}^{(C-1)}$  be a column vector, storing independently modeled probabilities among non-target classes (*i.e.*, without considering the  $k$ -th class). The conventional LD uses the KL divergence [9] between the output probabilities  $\hat{\mathbf{p}}^T$  and  $\hat{\mathbf{p}}^S$  of a teacher and a student network, respectively. Its loss function is expressed as follows<sup>1</sup>:

$$\text{LD} = \text{KL}(\hat{\mathbf{p}}^T \| \hat{\mathbf{p}}^S) = \hat{p}_k^T \log \frac{\hat{p}_k^T}{\hat{p}_k^S} + \sum_{i=1, i \neq k}^C \hat{p}_i^T \log \frac{\hat{p}_i^T}{\hat{p}_i^S}, \quad (1)$$

<sup>1</sup> $\mathcal{T}$  and  $\mathcal{S}$  denote teacher and student DNN models, respectively.

which can be reformulated as follows [22]:

$$\begin{aligned} \text{LD} = & \underbrace{\hat{p}_k^T \log \frac{\hat{p}_k^T}{\hat{p}_k^S} + (1 - \hat{p}_k^T) \log \frac{1 - \hat{p}_k^T}{1 - \hat{p}_k^S}}_{\text{KL}(\mathbf{b}^T \parallel \mathbf{b}^S)} \\ & + (1 - \hat{p}_k^T) \underbrace{\sum_{i=1, i \neq k}^C \hat{p}_{i, \setminus k}^T \log \frac{\hat{p}_{i, \setminus k}^T}{\hat{p}_{i, \setminus k}^S}}_{\text{KL}(\hat{\mathbf{p}}_{\setminus k}^T \parallel \hat{\mathbf{p}}_{\setminus k}^S)}. \end{aligned} \quad (2)$$

(2) can be rewritten as follows:

$$\text{LD} = \underbrace{\text{KL}(\mathbf{b}^T \parallel \mathbf{b}^S)}_{\text{TCLD}} + (1 - \hat{p}_k^T) \underbrace{\text{KL}(\hat{\mathbf{p}}_{\setminus k}^T \parallel \hat{\mathbf{p}}_{\setminus k}^S)}_{\text{NCLD}}, \quad (3)$$

where the TCLD term represents the similarity between  $\mathbf{b}^T$  and  $\mathbf{b}^S$ , while the NCLD term denotes the similarity between  $\hat{\mathbf{p}}_{\setminus k}^T$  and  $\hat{\mathbf{p}}_{\setminus k}^S$ . Obviously, both TCLD and the weight of NCLD terms are related to  $\hat{p}_k^T$ , making them coupled. As  $(1 - \hat{p}_k^T)$  is often much smaller than the weight of TCLD term (consistently 1), the effects of NCKD term are often suppressed. However, in [22], the authors claimed that the primary contribution of LD comes from NCLD term, and reformulated (3) as follows:

$$\text{DKD} = \alpha \text{TCLD} + \beta \text{NCLD}. \quad (4)$$

The two independent hyper-parameters  $\alpha$  and  $\beta$  are used to balance the TCLD and NCLD terms. Extensive experiments conducted across a variety of training datasets demonstrate that setting  $\alpha$  to 1, as consistent with (3), and assigning  $\beta$  positive integer values between 1 and 10 results in improved distillation performance compared to conventional LD. Nevertheless, upon revisiting (3), it becomes evident that  $(1 - \hat{p}_k^T)$  at each pixel varies independently. Thus, we aim to dynamically control the weight of the NCLD term across logits.

A logit value  $z_k^S$  approaching infinity indicates high confidence in the classification of  $\mathbf{q}$ . This implies that ambiguity arises in the student DNN model, when  $z_k^S$  is not sufficiently high. Differentiating DKD with respect to  $z_k^S$  yields the following expression:

$$\begin{aligned} \frac{\partial \text{DKD}}{\partial z_k^S} &= \alpha \frac{\partial \text{TCLD}}{\partial z_k^S} + \beta \frac{\partial \text{NCLD}}{\partial z_k^S} \\ &= -\alpha \left( \frac{\hat{p}_k^T}{\hat{p}_k^T} \frac{\partial \hat{p}_k^T}{\partial z_k^S} + \frac{(1 - \hat{p}_k^T)}{(1 - \hat{p}_k^S)} \frac{\partial \hat{p}_k^T}{\partial z_k^S} \right) + 0, \end{aligned} \quad (5)$$

which reveals that the gradient of the DKD loss is only related to TCLD, with no dependence on NCLD. However, as discussed earlier, it is essential to pay more attention to NCLD, especially when the student network is less confident. Therefore, we are motivated to introduce the confidence of the student’s logits, as measured by their probability entropy, to dynamically balance TCLD and NCLD.

**Dynamic Weight Controller.** A thorough search of the relevant literature reveals no discussions on the adaptive control of the NCLD weight. We were inspired by a recent study [32] that discussed setting adaptive temperature in graph neural networks for knowledge distillation. We assign each logit with

an adaptive NCLD weight  $\beta$  based on both the probability vector  $\hat{\mathbf{p}}$  and the confidence measure  $c = -\hat{\mathbf{p}}^T \log \hat{\mathbf{p}}$  at the given pixel  $\mathbf{q}$ . Expanding to the entire logit tensor  $\mathbf{Z}^S \in \mathbb{R}^{C \times H \times W}$  generated by the student model, we first compute the confidence vector  $\mathbf{c}^S \in \mathbb{R}^{HW}$  for all pixels using the following expression:

$$\mathbf{c}^S = -\left(\hat{\mathbf{P}}^S \odot \log \hat{\mathbf{P}}^S\right) \mathbf{1}_C, \quad (6)$$

where  $\odot$  represents element-wise dot product between two matrices,  $\mathbf{1}_C$  is a  $C$ -entry column vector of ones, ‘‘Reshape’’ operation denotes expanding a three-dimensional tensor into a two-dimensional matrix and  $\hat{\mathbf{P}}^S \in \mathbb{R}^{HW \times C}$  is a matrix calculated as follows:

$$\hat{\mathbf{P}}^S = \text{Reshape}\left(\text{Softmax}\left(\mathbf{Z}^S\right)\right). \quad (7)$$

$\beta^S \in \mathbb{R}^{HW \times C}$  is a matrix storing the NCLD weights with fixed range  $[\beta_{\min}, \beta_{\max}]$ . It is subsequently obtained as follows:

$$\begin{aligned} \beta^S &= (\beta_{\max} - \beta_{\min}) \text{Sigmoid}\left(\text{MLP}\left(\Omega^S\right)\right) \\ &+ \beta_{\min} \mathbf{1}_{HW} \mathbf{1}_C^T, \end{aligned} \quad (8)$$

where

$$\Omega^S = \text{Concat}\left(\hat{\mathbf{P}}^S, \mathbf{c}^S\right), \quad (9)$$

and ‘‘Concat’’ represents the operation to concatenate the matrix  $\hat{\mathbf{P}}^S \in \mathbb{R}^{HW \times C}$  and the confidence vector  $\mathbf{c}^S \in \mathbb{R}^{HW}$  to obtain  $\Omega^S \in \mathbb{R}^{HW \times (C+1)}$ . Through extensive experiments detailed in Sect. IV-F, we first validate the effectiveness of our proposed DWC, when  $\Omega^S = \hat{\mathbf{P}}^S$ . Moreover, it achieves improved performance, when further incorporating  $\mathbf{c}^S$  into  $\Omega^S$ . Specifically, let  $\mathbf{T}^S \in \mathbb{R}^{HW \times C}$  and  $\mathbf{N}^S = \mathbf{1}_{HW} \mathbf{1}_C^T - \mathbf{T}^S \in \mathbb{R}^{HW \times C}$  be the target and non-target ground-truth matrices in a Boolean format, where each row is a binary vector corresponding to the given segmentation ground truth. Therefore, extending (4) to the entire image results in the logit distillation loss as follows:

$$\begin{aligned} \mathcal{L}_L &= \alpha \underbrace{\mathbf{1}_{(HW)}^T \left( \mathbf{B}^S \odot \log \left( \mathbf{B}^T \oslash \mathbf{B}^S \right) \right) \mathbf{1}_2}_{\text{TCLD}} \\ &+ \mathbf{1}_{(HW)}^T \underbrace{\left( \beta^S \odot \hat{\mathbf{P}}_{\setminus k}^S \odot \log \left( \hat{\mathbf{P}}_{\setminus k}^T \oslash \hat{\mathbf{P}}_{\setminus k}^S \right) \right) \mathbf{1}_C}_{\text{logit-wise-weighted NCLD}}, \end{aligned} \quad (10)$$

where  $\oslash$  denotes element-wise division,

$$\mathbf{B}^{T,S} = \text{Concat}\left(\hat{\mathbf{P}}^{T,S} \odot \mathbf{T}^{T,S} \mathbf{1}_C, \hat{\mathbf{P}}^{T,S} \odot \mathbf{N}^{T,S} \mathbf{1}_C\right) \quad (11)$$

is a tensor of size  $\mathbb{R}^{HW \times 2}$  storing the binary probabilities at each pixel,

$$\hat{\mathbf{P}}_{\setminus k}^{T,S} = \frac{\exp\left(\text{Reshape}\left(\mathbf{Z}^{T,S}\right) - \delta \mathbf{T}^{T,S}\right)}{\exp\left(\text{Reshape}\left(\mathbf{Z}^{T,S}\right) - \delta \mathbf{T}^{T,S}\right) \mathbf{1}_C \mathbf{1}_C^T} \quad (12)$$

is a tensor of size  $\mathbb{R}^{HW \times C}$  storing the independently modeled probabilities among non-target classes at each pixel, and  $\delta$  is a large value approaching infinity. Compared with (4), the

inclusion of the variable  $\beta^S$  in (10) allows each non-target class logit in the output to receive an adaptive weight that adjusts during the training process, thereby enhancing the overall performance of LD. The comprehensive quantitative comparison between DKD [22] and our proposed DWC-based LD is provided in Sect. IV-C.

### B. Adaptively-Recalibrated Feature Distillation

The above-mentioned logit distillation method relies exclusively on the output of the last layer, overlooking the significance of intermediate-level features within both the teacher and student DNN models. It has nevertheless been demonstrated that these features plays a critical role in effective representation learning, especially in very deep neural networks [31]. Therefore, we design an adaptively-recalibrated feature distillation approach to further boost the transfer of spatial geometric prior knowledge from the teacher model to the student model. The remainder of this subsection details a feature recalibration process using kernel regression and a comprehensive feature consistency measurement method leveraging CKA [23] based on the HSIC [24].

**Feature Recalibration via Kernel Regression.** Let the feature maps produced by the teacher and student DNN models be the tensors  $\mathbf{F}^T \in \mathbb{R}^{C^T \times H^T \times W^T}$  and  $\mathbf{F}^S \in \mathbb{R}^{C^S \times H^S \times W^S}$ , respectively. Following the previous studies [18], [33]–[35], we first align tensors  $\mathbf{F}^T$  and  $\mathbf{F}^S$  and produce matrix  $\mathbf{F}_a^{T,S}$  through the following process:

$$\mathbf{F}_a^{T,S} = \text{ReLU} \left( \text{Norm} \left( \text{Conv}_{3 \times 3}(\text{Reshape}(\mathbf{F}^{T,S})) \right) \right), \quad (13)$$

where  $\mathbf{F}_a^{T,S} \in \mathbb{R}^{C^T \times HW}$ , and  $HW = \min H^{T,S} \min W^{T,S}$ . We take into account both spatial and channel alignment, given the specific nature of our task, where the feature maps from a single encoder and a duplex encoder differ significantly in the channel dimension.

Before delving into feature distillation, a pertinent question arises: are the features, having undergone alignment to a common shape using (13), ready for utilization? Extensive quantitative and qualitative experimental results lead us to a negative conclusion. We attribute the unsatisfactory performance of feature distillation to the discrepancy in feature scales and distributions between the teacher and student feature maps. On one hand, features often exhibit variations in different orders of magnitude, making their direct comparisons difficult [15], [16]. Working directly with the aligned features  $\mathbf{F}_a^T$  and  $\mathbf{F}_a^S$  could result in consistency measures being dominated by the model with large magnitude features. On the other hand, the absolute density of the data may vary significantly, or the shape of feature clusters may also vary with locality [21]. Thus, recalibrating feature map distributions becomes another critical aspect that demands further attention. In particular, in our research problem, the teacher DNN model learns heterogeneous features from both RGB images and spatial geometric information, while the student model is exclusively exposed to RGB images. Such a substantial difference in the learning data format exacerbates the knowledge transfer challenges. Taking inspiration from the knowledge transfer

algorithm introduced in [14], which utilizes kernel regression to minimize the maximum mean discrepancy between teacher and student feature map probability distributions, we apply this technique to recalibrate the aligned features in our specific problem. Such a feature recalibration process named Laplace-based kernel regression can be formulated as follows:

$$\mathbf{F}_k^{T,S} = \text{EXP} \left( -\frac{(\mathbf{F}_a^{T,S} - \bar{\mathbf{F}}_a^{T,S}) \odot (\mathbf{F}_a^{T,S} - \bar{\mathbf{F}}_a^{T,S})}{\sigma} \right), \quad (14)$$

where ‘‘EXP’’ represents the operation to take the exponent for each element in the matrix, and

$$\bar{\mathbf{F}}_a^{T,S} = \frac{1}{H \times W \times C^T} \mathbf{1}_{C^T}^\top \mathbf{F}_a^{T,S} \mathbf{1}_{HW}. \quad (15)$$

The other kernel regression approaches utilized in our study are expressed in detail as follows:

- Linear-based kernel regression:

$$\mathbf{F}_k^{T,S} = \mathbf{F}_a^{T,S} - \bar{\mathbf{F}}_a^{T,S}. \quad (16)$$

- Gaussian-based kernel regression:

$$\mathbf{F}_k^{T,S} = \text{EXP} \left( -\frac{(\mathbf{F}_a^{T,S} - \bar{\mathbf{F}}_a^{T,S}) \odot (\mathbf{F}_a^{T,S} - \bar{\mathbf{F}}_a^{T,S})}{2\sigma^2} \right), \quad (17)$$

where  $\sigma^2$  is empirically set to the mean of the squared distances between  $\mathbf{F}_a^{T,S}$  and  $\bar{\mathbf{F}}_a^{T,S}$  [14].

The comprehensive comparisons with two other common kernel regression methods (linear-based and Gaussian-based) are given in Sect. IV-G.

**Feature Consistency Measurement.** As mentioned above, measuring the consistency (or similarity) between intermediate features in teacher and student DNN models is the key to feature distillation. Although Euclidean distance, cosine similarity, and the Pearson correlation coefficient can all serve this purpose, it has been witnessed that CKA [23] based on the HSIC [24] provides a more comprehensive quantification of representational consistency, as demonstrated in several fundamental machine learning studies [23], [36], [37].

We begin by computing two Gram matrices  $\mathbf{T}_k = \mathbf{F}_k^T \mathbf{F}_k^{T^\top} \in \mathbb{R}^{C^T \times C^T}$  and  $\mathbf{S}_k = \mathbf{F}_k^S \mathbf{F}_k^{S^\top} \in \mathbb{R}^{C^S \times C^S}$ , reflecting the similarities between pairs of examples based on the representations contained in  $\mathbf{F}_k^T$  and  $\mathbf{F}_k^S$  [23]. Their HSIC measure is subsequently computed as follows [24]:

$$\text{HSIC}(\mathbf{T}_k, \mathbf{S}_k) = \frac{C^{T^2}}{(C^T - 1)^2} \left( \text{tr}(\mathbf{S}_k \mathbf{T}_k) + \frac{\mathbf{1}_{C^T}^\top \mathbf{S}_k \mathbf{1}_{C^T} \mathbf{1}_{C^T}^\top \mathbf{T}_k \mathbf{1}_{C^T}}{C^{T^2}} - \frac{2}{C^{T^2}} \mathbf{1}_{C^T}^\top \mathbf{S}_k \mathbf{T}_k \mathbf{1}_{C^T} \right), \quad (18)$$

which statistically quantifies the dependences between  $\mathbf{T}_k$  and  $\mathbf{S}_k$ . CKA further normalizes the HSIC measures using the following expression:

$$\text{CKA}(\mathbf{T}_k, \mathbf{S}_k) = \frac{\text{HSIC}(\mathbf{T}_k, \mathbf{S}_k)}{\sqrt{\text{HSIC}(\mathbf{T}_k, \mathbf{T}_k) \text{HSIC}(\mathbf{S}_k, \mathbf{S}_k)}}. \quad (19)$$

A CKA measure approaching 1 indicates that the intermediate features in the teacher and student DNN models tend to be

consistent. In our task, this suggests that the spatial geometric prior knowledge learned by the data-fusion teacher networks at the feature level is likely to have been implicitly infused into the single-modal student network. Therefore, the feature distillation loss can be formulated as follows:

$$\mathcal{L}_F = \sum_{n=1}^N (1 - \text{CKA}(\mathbf{T}_{k,n}, \mathbf{S}_{k,n})), \quad (20)$$

where  $\mathbf{T}_{k,n}$  and  $\mathbf{S}_{k,n}$  are yielded using the  $n$ -th pair of recalibrated teacher and student feature maps, respectively, and  $N$  denotes the total number of feature maps. The quantitative comparisons of the above-mentioned feature consistency measurement methods are provided in Sect. IV-G.

### C. Overall Loss

As depicted in Fig. 1, our proposed LIX framework distills a teacher duplex-encoder (RGB-X) DNN architecture into a student DNN fed with only RGB images by two critical methods: DWLD and ARFD. DWLD first reformulates the classical KD loss into two independent and decoupled terms: TCLD and NCLD. Subsequently, a dynamic weight controller utilizing MLP layers generates a weight for each logit adaptively. Therefore, TCLD and weighted NCLD terms together form the LD loss  $\mathcal{L}_L$ . As for FD, we first utilize adaptive feature alignment and recalibration approaches based on kernel regression, which recalibrate the feature map distributions of the teacher and student DNN models across various dimensions. Subsequently, we measure the similarity between intermediate features to formulate our novel FD loss  $\mathcal{L}_F$  in teacher and student DNN models based on CKA algorithm, which quantifies the feature consistency between the teacher and student DNN models.

Summarily, the overall loss function can be formulated as a combination of the initial loss  $\mathcal{L}_H$  of the hard labels (ground truth) and distillation losses, consisting of a logit distillation loss  $\mathcal{L}_L$  and a feature distillation loss  $\mathcal{L}_F$ , as follows:

$$\mathcal{L} = \mathcal{L}_H + \lambda_L \mathcal{L}_L + \lambda_F \mathcal{L}_F, \quad (21)$$

where  $\lambda_L$  and  $\lambda_F$  are hyper-parameters used to balance  $\mathcal{L}_L$  and  $\mathcal{L}_F$ , respectively. The selection of  $\lambda_L$  and  $\lambda_F$  are detailed in the sec. IV-H. By minimizing (21), the student DNN model with a single encoder can be implicitly infused the spatial geometric prior knowledge learned by the teacher DNN model with a duplex encoder.

## IV. EXPERIMENTS

### A. Experimental Setup

Datasets. We utilize two public datasets to evaluate the performance of our proposed methods: the vKITTI2 dataset [38] (synthetic yet large-scale) and the KITTI Semantics dataset [39] (real-world yet modest-scale). Their details are as follows:

- The **vKITTI2 dataset** contains virtual replicas of five sequences from the KITTI dataset and provides semantic annotations for 15 different classes. Dense ground-truth depth maps are acquired through depth rendering using a virtual engine. In our experiments, we randomly select

TABLE I  
PERFORMANCE OF TEACHER DNN MODELS TRAINED USING DIFFERENT “X” DATA.

Dataset	“X” Data	mFsc (%) $\uparrow$	fwFsc (%) $\uparrow$	mIoU (%) $\uparrow$	fwIoU (%) $\uparrow$
vKITTI2	Depth	97.35	98.23	94.96	98.19
	Disp	<b>97.72</b>	<b>99.12</b>	<b>95.63</b>	<b>98.27</b>
	Normal	97.09	98.02	94.48	97.84
	HHA	97.38	98.34	95.01	98.25
KITTI Semantic	Depth	<b>74.79</b>	<b>93.47</b>	<b>64.78</b>	88.25
	Disp	74.38	92.88	63.86	<b>88.90</b>
	Normal	67.62	89.76	54.31	86.29
	HHA	73.25	91.02	61.77	88.21
CityScapes	Depth	48.44	78.46	37.28	77.30
	Disp	<b>49.83</b>	<b>79.93</b>	<b>38.53</b>	<b>78.96</b>
	Normal	46.79	76.86	36.04	75.95
	HHA	45.23	72.36	34.54	72.89

1,500 images from this dataset, along with their semantic and depth annotations, to validate the effectiveness of our proposed logit and feature distillation approaches. These images are randomly divided into a training set, a validation set, and a test set, with a ratio of 6:1:3.

- The **KITTI Semantics dataset** contains 200 real-world images captured in various driving scenarios. It provides ground-truth semantic annotations for 19 different classes (in alignment with the Cityscapes [8] dataset). Sparse disparity ground truth is obtained using a Velodyne HDL-64E LiDAR. We generate dense depth maps using a well-trained CreStereo [40] model in the experiments. These images are randomly divided into a training set and a validation set, with a ratio of 7:3.

Implementation Details and Evaluation Metrics. Our experiments are conducted on an NVIDIA RTX 3090 GPU. All images are resized to  $1,248 \times 384$  pixels before being fed into the network. We utilize the stochastic gradient descent (SGD) [41] optimizer for model training, with momentum and weight decay parameters set to 0.9 and  $5 \times 10^{-4}$ , respectively. The initial learning rate is set to  $1 \times 10^{-2}$ , and training is conducted for 500 epochs with early stopping used to prevent over-fitting. Standard data augmentation techniques are applied to enhance the model’s robustness. We employ four metrics to quantify the performance of the KD algorithms: the mean and frequency-weighted F1-score (abbreviated as mFsc and fwFsc, respectively) and the mean and frequency-weighted intersection over union (abbreviated as mIoU and fwIoU, respectively).

### B. Performance of Teacher Models Trained Using Different “X” Data

In this subsection, we conduct experiments to evaluate the performance of teacher models with different “X” data as inputs. As shown in Table I, the best results are shown in bold font, with  $\uparrow$  signifying that higher values correspond to better performance. It is evident that the teacher model achieves superior performance when “X” data are depth or disparity images. This observation may be attributed to the introduction of noise from the height channel when using HHA maps, and the limited utility of surface normal information, which may be primarily useful for planar surface extraction. We also speculate that these unexpected results could be

TABLE II  
COMPARISON WITH SOTA KNOWLEDGE DISTILLATION APPROACHES ON THE vKITTI2 AND KITTI SEMANTICS DATASETS.

Network	KD Type	Algorithm	vKITTI2 Dataset				KITTI Semantic Dataset			
			mFsc (%) $\uparrow$	fwFsc (%) $\uparrow$	mIoU (%) $\uparrow$	fwIoU (%) $\uparrow$	mFsc (%) $\uparrow$	fwFsc (%) $\uparrow$	mIoU (%) $\uparrow$	fwIoU (%) $\uparrow$
SNE-RoadSeg	Baseline	Teacher Model	97.72	99.12	95.63	98.27	74.79	93.47	64.78	88.25
		Student Model	94.51	97.83	89.91	95.82	62.73	90.86	51.89	84.21
	LD	KD [9]	94.89	97.90	90.59	95.94	67.25	91.29	55.69	84.81
		CWKD [11]	95.02	97.95	90.82	96.03	64.22	90.90	52.94	84.28
		DKD [22]	94.97	97.94	90.75	95.97	65.89	90.83	54.57	84.10
		<b>DWLD (Ours)</b>	<b>95.42</b>	<b>98.06</b>	<b>91.50</b>	<b>96.24</b>	<b>71.43</b>	<b>92.51</b>	<b>60.28</b>	<b>86.72</b>
	FD	AT [12]	94.61	97.87	90.12	95.89	65.24	<b>91.34</b>	54.44	85.38
		FitNet [31]	94.89	97.92	90.59	95.99	<b>68.23</b>	90.86	50.86	84.21
		FT [13]	94.75	97.91	90.34	95.97	63.98	90.80	52.95	84.10
		NST [14]	83.19	90.94	73.27	84.55	65.80	88.17	48.09	80.32
		RKD [15]	94.69	97.81	90.25	95.78	61.77	89.91	50.38	82.82
		SP [16]	95.08	97.96	90.93	96.06	66.39	90.92	<b>55.01</b>	84.30
		VID [17]	95.05	97.95	90.87	96.03	65.92	90.89	54.53	84.25
		<b>ARFD (Ours)</b>	<b>95.20</b>	<b>98.01</b>	<b>90.97</b>	<b>96.16</b>	68.08	91.30	54.52	<b>85.93</b>
LD+FD	<b>LIX (Ours)</b>	<b>95.79</b>	<b>98.23</b>	<b>91.95</b>	<b>96.33</b>	<b>71.93</b>	<b>92.91</b>	<b>60.33</b>	<b>87.32</b>	
MFNet	Baseline	Teacher Model	92.65	97.68	86.96	95.57	55.53	88.86	44.92	81.34
		Student Model	91.22	96.93	84.59	94.19	45.46	82.79	35.39	73.15
	LD	KD [9]	91.93	97.06	85.70	94.42	42.65	81.58	33.15	71.75
		CWKD [11]	91.63	97.02	85.29	94.36	45.38	82.91	35.53	73.40
		DKD [22]	91.68	97.06	85.29	94.42	42.22	81.21	32.83	71.28
		<b>DWLD (Ours)</b>	<b>92.29</b>	<b>97.22</b>	<b>85.94</b>	<b>94.68</b>	<b>45.55</b>	<b>83.62</b>	<b>36.23</b>	<b>74.71</b>
	FD	AT [12]	91.97	97.13	85.78	94.55	40.85	80.05	31.59	69.72
		FitNet [31]	91.36	96.93	84.83	94.19	44.00	81.77	34.00	71.98
		FT [13]	91.47	96.96	84.96	94.25	43.92	82.84	34.66	73.34
		NST [14]	89.39	96.58	81.88	93.58	46.26	83.82	35.97	74.61
		RKD [15]	85.33	95.44	76.19	91.66	<b>64.99</b>	67.74	17.15	55.87
		SP [16]	91.98	97.10	85.78	94.50	46.35	83.51	36.16	74.22
		VID [17]	91.78	97.01	85.54	94.34	43.41	80.97	33.70	70.89
		<b>ARFD (Ours)</b>	<b>92.46</b>	<b>97.27</b>	<b>86.52</b>	<b>94.80</b>	47.32	<b>84.53</b>	<b>37.10</b>	<b>75.23</b>
LD+FD	<b>LIX (Ours)</b>	<b>92.50</b>	<b>97.32</b>	<b>86.88</b>	<b>95.10</b>	47.41	<b>84.62</b>	<b>37.33</b>	<b>75.36</b>	

attributed to the greater preservation of raw spatial geometry information in depth and disparity images, compared to HHA and surface normal maps. Eventually, we opt to use the teacher model trained with depth or disparity images for subsequent distillation experiments.

### C. Comparison with State-of-the-Art Methods

As illustrated in Fig. 2, LIX on the KITTI Semantic datasets consistently outperforms other KD methods, demonstrating its capacity to infuse prior spatial geometric knowledge through the combined use of DWLD and ARFD. This advantage is particularly pronounced in situations where RGB features alone are less informative. However, it is important to note that the student DNN model may encounter challenges in handling fine-grained details in complex scenarios, such as distinguishing between traffic lights and traffic signs.

The quantitative experimental results on the vKITTI2 and KITTI Semantic datasets are presented in Table II. In our baseline experiments, the teacher model uses a duplex encoder to learn semantic segmentation from RGB-D data, while the student model uses a single encoder to learn semantic segmentation exclusively from RGB images. These results suggest that our proposed DWLD and ARFD algorithms outperform all other SoTA LD and FD algorithms, respectively, on the vKITTI2 dataset. When DWLD is utilized solely for our specific task, we observe significant improvements compared to the baseline student model, which is trained exclusively on RGB images using a single encoder to learn semantic

segmentation, without the incorporation of any LD algorithm. These results serve as strong evidence for the effectiveness and superior performance of our proposed DWLD algorithm. We arrive at a similar conclusion when evaluating the performance of ARFD. However, it achieves comparable performance when using MFNet and significantly better performance when using SNE-RoadSeg on the KITTI Semantics dataset. LIX, the combined use of these two algorithms enables the student DNN model with a single encoder to achieve comparable performance to that of the teacher model with a duplex encoder. This demonstrates the viability of our proposed KD strategy for implicit infusion of spatial geometric prior knowledge.

Moreover, we observe that KD performance is significantly influenced by the model parameters as well as the difficulty level of the dataset. The encoders of the teacher and student SNE-RoadSeg models have 116.28 M and 58.14 M parameters, respectively, while the encoders of the teacher and student MFNet models have 0.60 M and 0.52 M parameters, respectively. To provide a more detailed analysis, Table II can be divided into four sections: (1) SNE-RoadSeg on the vKITTI2, (2) SNE-RoadSeg on the KITTI Semantics, (3) MFNet on the vKITTI2, and (4) MFNet on the KITTI Semantics. Since vKITTI2 is larger and less challenging, DWLD, ARFD, and LIX all achieve the SoTA performance regardless of the model parameters. When our method is applied to MFNet, its performance is on par with that of the teacher network on the vKITTI2 dataset, demonstrating superior effectiveness compared to SNE-RoadSeg with LIX. We attribute this superior

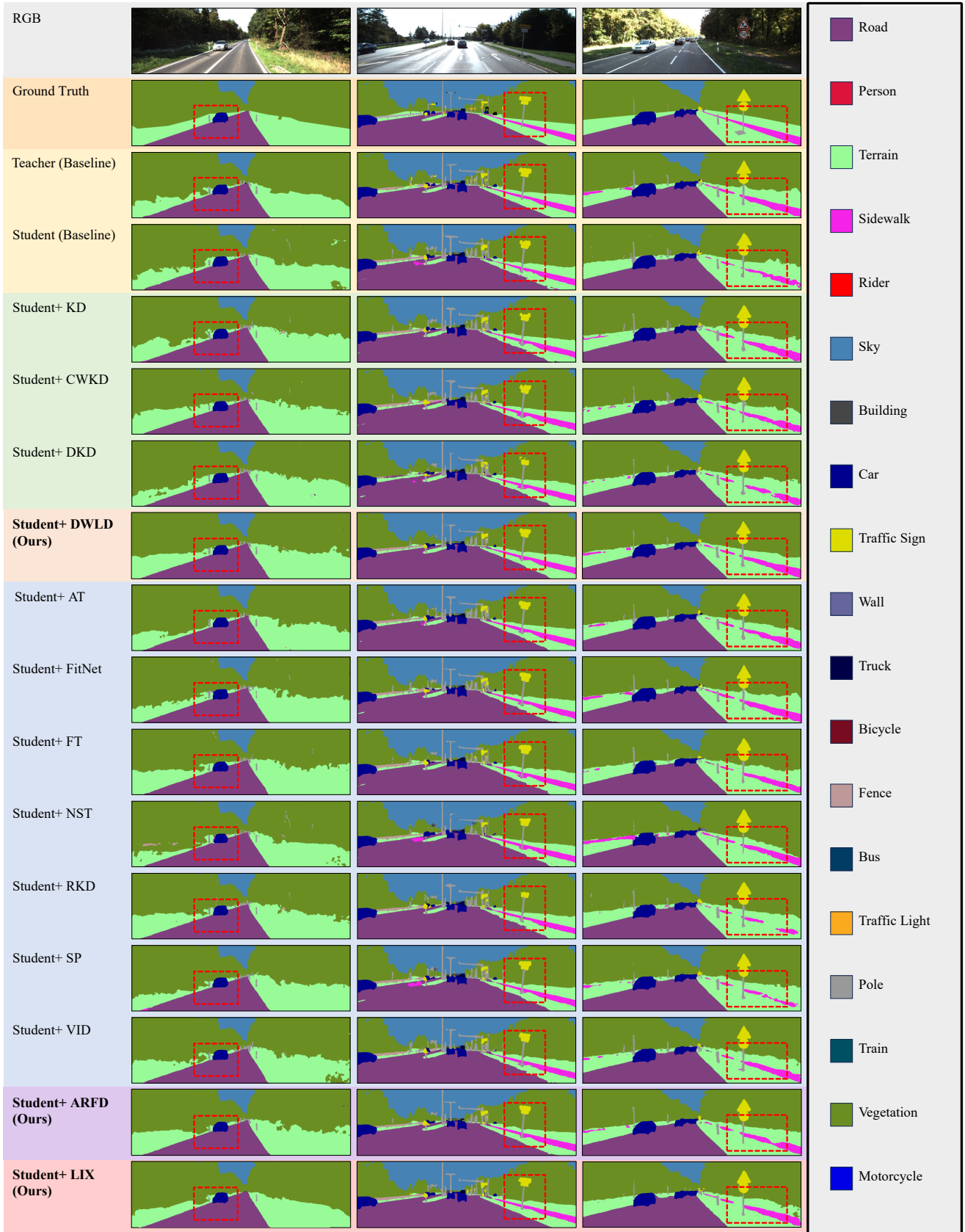


Fig. 2. Qualitative comparison with other SoTA KD approaches, where the significantly improved areas are highlighted with red dashed boxes.

performance not only to the comparable parameter numbers between the teacher and student MFNet networks but also to

the lower difficulty level of the dataset. It is possible that the lightweight MFNet is adequately capable of learning semantic



TABLE III  
COMPARISON WITH SOTA KD APPROACHES WHEN USING OFF-NET AS THE BASELINE MODEL.

KD Type	Algorithm	LIX on OFF-Net			
		mFsc (%)	fwFsc (%)	mIoU (%)	fwIoU (%)
Baseline	Teacher Model	65.25	91.22	48.19	84.78
	Student Model	47.97	82.80	36.48	72.58
LD	KD [9]	46.25	78.98	33.10	70.21
	CWKD [11]	52.43	84.79	40.12	75.17
	DKD [22]	52.93	84.89	40.73	75.31
	<b>DWLD (Ours)</b>	<b>62.20</b>	<b>86.20</b>	<b>45.84</b>	<b>80.42</b>
FD	AT [12]	46.34	79.09	32.51	67.78
	FitNet [31]	47.67	82.56	36.18	72.31
	FT [13]	47.12	75.51	32.47	62.76
	NST [14]	51.53	84.39	39.38	74.53
	RKD [15]	47.89	76.01	33.00	63.30
	SP [16]	56.52	86.81	43.97	78.00
	VID [17]	60.41	87.68	<b>47.37</b>	79.19
	<b>ARFD (Ours)</b>	<b>60.42</b>	<b>88.01</b>	43.25	<b>80.02</b>
LD+FD	<b>LIX (Ours)</b>	<b>62.87</b>	<b>88.02</b>	<b>48.98</b>	<b>81.29</b>

segmentation on this less challenging dataset.

On the other hand, the experimental results on the KITTI Semantics dataset have exceeded our expectations, when using SNE-RoadSeg in conjunction with our method. ARFD outperforms other algorithms only in fwIoU and achieves performance comparable to that of the SoTA algorithms when evaluated using other metrics. We believe that this may be attributed to a “mismatch” between SNE-RoadSeg and the KITTI Semantics dataset, where a large model is trained on a relatively small dataset, potentially leading to over-fitting. Even though the smaller MFNet yields lower quantitative results on this dataset, we believe that its teacher model contains less irrelevant information. This reduced noise in the teacher model may prevent the student DNN model from being misled into learning the implicit infusion of spatial geometric prior knowledge.

#### D. Applying LIX to Transformer

Recently, [42] presented a Transformer-based RGB-X semantic segmentation network, referred to as OFF-Net, which utilizes two SegFormer [43] encoders to extract heterogeneous features. In this subsection, we utilize this network to further validate the compatibility of our proposed LIX framework with Transformer-based architectures.

The quantitative experimental results on the KITTI Semantics datasets are presented in Table III. These results indicate that our proposed dynamically-weighted logit distillation (DWLD) and ARFD outperform all other SoTA logit distillation and feature distillation algorithms, respectively. When DWLD is exclusively applied to our specific task, significant improvements are observed compared to the baseline student model. These results provide additional evidence for the effectiveness and superior performance of our proposed DWLD algorithm on a Transformer-based architecture. Similar conclusions are drawn when evaluating the performance of ARFD. LIX, through the combined use of these two algorithms, enables the student model with a single encoder to achieve comparable performance to that of the teacher model with a duplex encoder. As expected, this affirms the effectiveness of our proposed LIX for the implicit infusion of

TABLE IV  
COMPARISON WITH SOTA KD APPROACHES ON THE CITYSCAPES DATASET.

KD Type	Algorithm	LIX on CityScapes			
		mFsc (%)	fwFsc (%)	mIoU (%)	fwIoU (%)
Baseline	Teacher Model	49.83	79.93	38.53	78.96
	Student Model	36.50	63.90	24.49	54.65
LD	KD [9]	36.90	61.49	24.58	51.72
	CWKD [11]	35.44	68.14	26.10	60.28
	DKD [22]	37.89	67.70	25.73	59.99
	<b>DWLD (Ours)</b>	<b>37.95</b>	<b>68.02</b>	<b>26.13</b>	<b>60.30</b>
FD	AT [12]	36.01	66.27	24.44	57.77
	FitNet [31]	37.47	65.39	25.31	56.42
	FT [13]	37.39	63.70	24.95	54.18
	NST [14]	38.23	69.06	26.02	51.51
	RKD [15]	37.25	65.44	24.28	54.17
	SP [16]	36.41	66.45	24.73	57.94
	VID [17]	36.75	65.92	24.66	57.28
<b>ARFD (Ours)</b>	<b>38.34</b>	<b>69.20</b>	<b>26.12</b>	<b>58.92</b>	
LD+FD	<b>LIX (Ours)</b>	<b>38.36</b>	<b>69.23</b>	<b>26.25</b>	<b>60.42</b>

spatial geometric prior knowledge into the student model. It becomes an intriguing avenue for future research to delve into the development of knowledge distillation methods specifically for Transformer-based models.

#### E. Performance of the LIX Framework on the CityScapes Dataset

To further validate the effectiveness of our proposed LIX framework on large-scale, real-world datasets, especially when the “X” data are noisy, we conduct additional experiments on the CityScapes dataset [8], which provides 2,975 pairs of training images and 500 pairs of validation images, all annotated with semantic labels. However, these images lack depth/disparity ground truth.

As shown in Table IV, our LIX framework demonstrates superior performance compared to all other knowledge distillation (KD) methods on the CityScapes dataset. These results further underscore the robustness and generalization ability of our approach in real-world autonomous driving scenarios. Nevertheless, it is worth noting an interesting observation during our experiments. Despite the CityScapes dataset being considerably larger than the KITTI Semantics dataset, the baseline model’s performance on CityScapes is degraded compared to its performance on KITTI Semantics. Additionally, the performance improvements achieved by the feature distillation (FD) methods are relatively less significant on the CityScapes dataset. This limitation may be attributed to inaccuracies in the “X” data, which can lead to a degradation in the effective feature extraction by the duplex encoders of the teacher network, ultimately hindering the infusion of accurate prior knowledge into the student model. Therefore, accurate spatial geometric information is not only foundational for RGB-X semantic segmentation but also crucial for effective knowledge transfer from teacher to student DNN models.

#### F. Ablation Study of Logit Distillation

We first compare DWLD with the baseline algorithm DKD, which requires a manually-set fixed  $\beta$ . As shown in Fig. 3(a), DWLD consistently demonstrates superior performance over DKD across different values of  $\beta$ , with an increase in

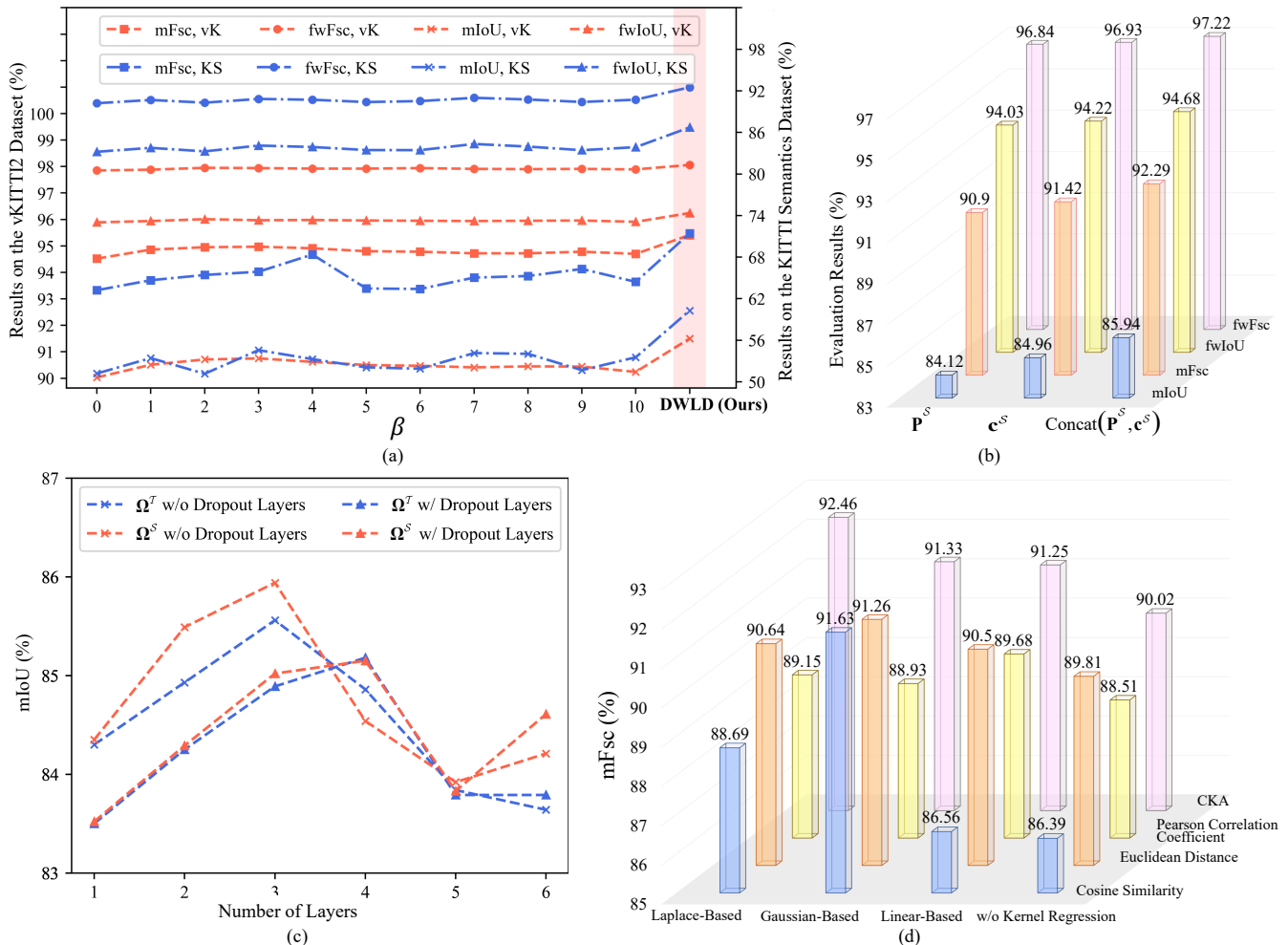


Fig. 3. Ablation study: (a) comparison between DKD and DWLD with respect to different  $\beta$ , where “vK” and “KS” are the abbreviations of “vKITTI2” and “KITTI Semantics”, respectively; (b) comparison among various designs of  $\Omega^S$  on the vKITTI2 dataset; (c) comparison among various designs of DWC; (d) comparisons of various kernel regression and feature consistency measurement methods on the vKITTI2 dataset.

mIoU by 0.79-1.47% on the vKITTI2 dataset and by 5.71-9.12% on the KITTI Semantics dataset. These results suggest that, compared to DKD, which sometimes struggles to find a proper single fixed weight  $\beta$ , our proposed DWLD offers a preferable option for both achieving better performance and simplifying the deployment process. Moreover, we validate the effectiveness of DWC when  $\Omega^S = \hat{P}^S$  and when  $c^S$  is further incorporated into  $\Omega^S$ . As depicted in Fig. 3(b), when  $\Omega^S = \text{Concat}(\hat{P}^S, c^S)$ , the student model achieves increases by 0.98%-1.82% in mIoU and by 0.87%-1.39% in mFsc, supporting our claim regarding the design of  $\Omega^S$ .

In theory, greater confidence in the teacher model should lead to better infusion of non-target class logit distillation (NCLD) information into the student model. While the design of the dynamic weight controller (DWC) draws inspiration from differentiating decoupled knowledge distillation (DKD) [22] concerning  $z_k^S$ , there remains a question as to whether the confidence of the teacher model also exerts a significant influence on DWC.

To address this question, we further validate the effectiveness of DWC using both  $\Omega^S$  and  $\Omega^T$  as inputs, with and without the incorporation of dropout layers, as illustrated in Fig. 3(c). As anticipated, DWC yields superior performance

when utilizing  $\Omega^S$  as input, confirming the fundamental practicability of the core concept underlying our DWC design.

Additionally, the inclusion of dropout layers does not appear to enhance the overall performance of DWC. For instance, when four MLP layers with dropout are employed, the neuron count is identical to that of the case where two MLP layers without dropout are used. However, the former demonstrates inferior performance.

Furthermore, Fig. 3(c) also provides readers with the quantitative results on the selection of MLP layers, which is another key aspect of our DWC design. It is evident that as the number of MLP layers increases, the performance of the student network shows a gradual improvement until it reaches a saturation point, after which its performance degrades due to over-fitting. Therefore, our DWC utilizes three MLP layers without dropout.

#### G. Ablation Study of Feature Distillation

As presented in Fig. 3(d), remarkable improvements are achieved through kernel regression with CKA for feature consistency measurement. These improvements can primarily be attributed to the effectiveness of kernel regression in reducing the gap between features in the teacher and student

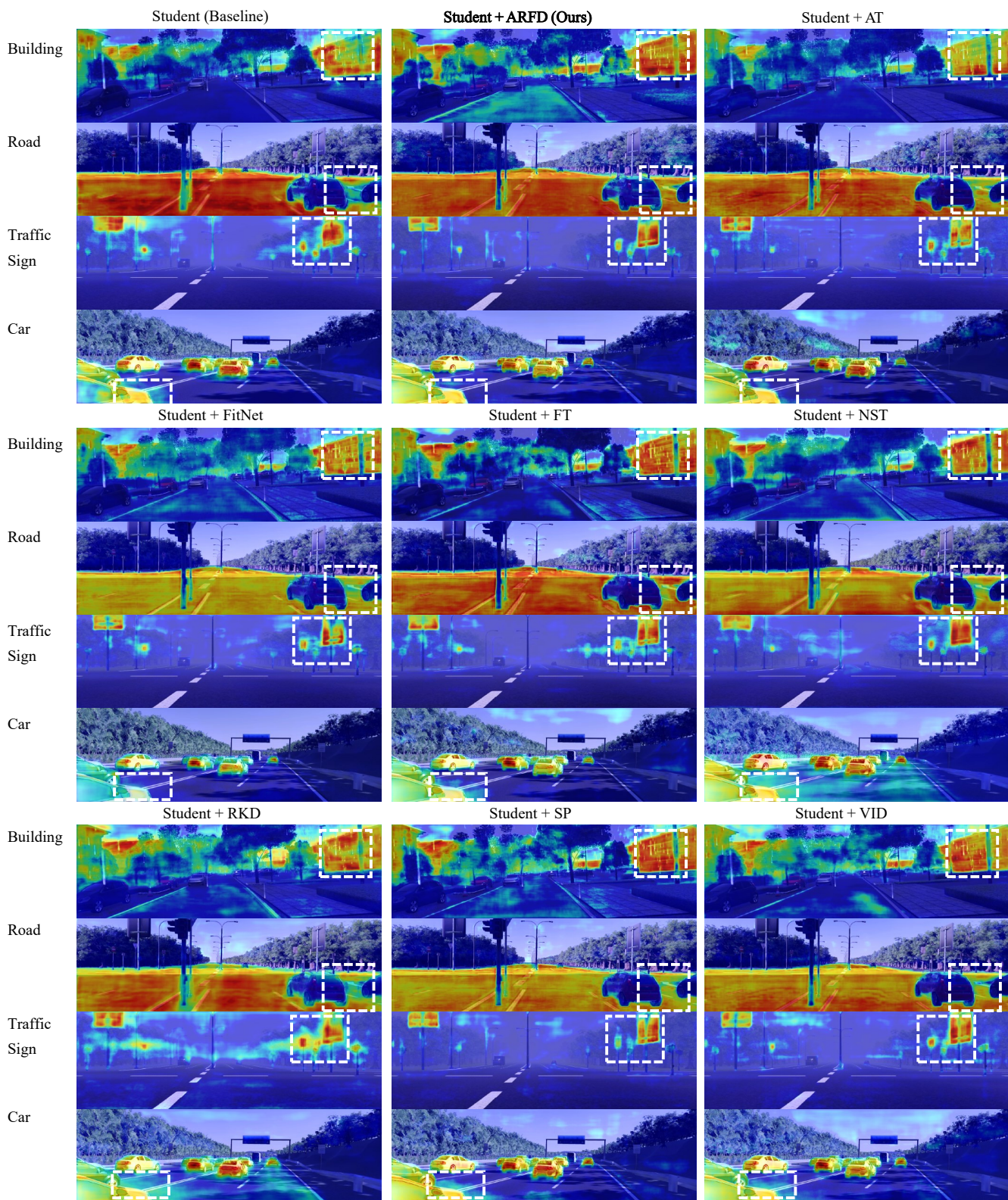


Fig. 4. Probabilities of different classes produced by the student DNN models, where the red and blue colors correspond to the high and low probability of the predictions, respectively, and the significantly improved areas are highlighted with white dashed boxes.

models across multiple dimensions. As expected, both Euclidean distance and the Pearson correlation coefficient prove effective for this purpose. However, when cosine similarity is used in conjunction with a linear kernel, it demonstrates even poorer performance, compared to the cases where no

kernel regression is employed. We posit that conventional similarity measurement methods such as cosine similarity have the opposite effect by aggregating the differences in attribute values. Consequently, these methods are susceptible to the influence of “noise” components from irrelevant attributes,

TABLE V  
LIX PERFORMANCE WITH RESPECT TO DIFFERENT RATIOS OF LOSS WEIGHTS.

Dataset	Ratio	mFsc (%) $\uparrow$	fwFsc (%) $\uparrow$	mIoU (%) $\uparrow$	fwIoU (%) $\uparrow$
vKITTI2	1:1:1	92.07	96.40	85.47	94.28
	1:2:1	91.97	96.70	86.05	94.39
	1:1:2	92.40	97.24	86.51	93.89
	2:1:1	<b>92.50</b>	<b>97.32</b>	<b>86.88</b>	<b>95.10</b>
KITTI Semantic	1:1:1	46.71	83.48	36.41	73.05
	1:2:1	46.28	84.31	36.36	72.32
	1:1:2	<b>47.40</b>	<b>84.60</b>	37.15	75.21
	2:1:1	47.32	84.53	<b>37.33</b>	<b>75.36</b>
CityScapes	1:1:1	37.25	68.32	25.43	58.32
	1:2:1	38.33	68.99	26.19	<b>60.50</b>
	1:1:2	38.29	69.21	<b>26.27</b>	60.38
	2:1:1	<b>38.36</b>	<b>69.23</b>	26.25	60.42

which can overshadow the similarity effects of numerous relevant attributes. In contrast, our ARFD, which leverages CKA based on the HSIC, offers a more comprehensive quantification of representational consistency. The optimal performance is achieved when combining Laplace-based kernel regression with CKA-based feature consistency measurement.

In this subsection, we also provide a qualitative comparison between our proposed ARFD and other state-of-the-art (SoTA) approaches. As depicted in Fig. 4, ARFD generates more confident predictions for each class. Notably, it leads to a more uniform distribution of probabilities for the wall and road classes in the student network’s predictions, indicating the effective infusion of spatial geometric prior knowledge through ARFD.

#### H. Weights for Different Losses

In this subsection, we conduct experiments to evaluate the performance of LIX with respect to different loss weights. We empirically set the ratios of the three losses to 1:1:1, 1:2:1, 1:1:2, and 2:1:1. While further hyper-parameter tuning is possible, it is important to consider the risk of over-fitting with limited data. As presented in Table V, our framework demonstrates insensitivity to the ratio of different losses, and “2:1:1” yields the best results across different datasets. This suggests that the prior knowledge of the teacher model serves primarily as an assistive role in helping the student model surpass its upper limit.

## V. CONCLUSION AND FUTURE WORK

This paper discussed a new computer vision problem: the implicit infusion of spatial geometric prior knowledge acquired by a duplex-encoder teacher DNN model into a single-encoder student DNN model. We contributed to both logit distillation and feature distillation by introducing the DWLD and the ARFD algorithms, respectively. We extend the DKD algorithm, by introducing a logit-wise dynamic weight controller, which assigns an appropriate weight to each logit. As for FD, we introduce two technical novelties: feature recalibration via kernel regression and in-depth feature consistency quantification via CKA. Through extensive experiments conducted with representative RGB-X semantic segmentation models on public autonomous driving datasets, we validate the effectiveness and superior performance of our developed LIX

framework, which combines DWLD and ARFD. Our future work will primarily concentrate on refining the designs of DWLD and ARFD for greater feasibility.

## REFERENCES

- [1] J. Li *et al.*, “RoadFormer: Duplex Transformer for rgb-normal semantic road scene parsing,” *arXiv preprint arXiv:2309.10356*, 2023. 1
- [2] R. Fan *et al.*, “SNE-RoadSeg: Incorporating surface normal information into semantic segmentation for accurate freespace detection,” in *Proceedings of the European Conference on Computer Vision (ECCV)*. Springer, 2020, pp. 340–356. 1, 2
- [3] J. Zhang *et al.*, “CMX: Cross-modal fusion for RGB-X semantic segmentation with transformers,” *IEEE Transactions on Intelligent Transportation Systems*, 2023. 1
- [4] B. Yin *et al.*, “DFormer: Rethinking RGBD representation learning for semantic segmentation,” *arXiv preprint arXiv:2309.09668*, 2023. 1
- [5] J. Zhang *et al.*, “Delivering arbitrary-modal semantic segmentation,” in *Proceedings of the IEEE/CVF Conference on Computer Vision and Pattern Recognition (CVPR)*, 2023, pp. 1136–1147. 1
- [6] Hazirbas *et al.*, “FuseNet: Incorporating depth into semantic segmentation via fusion-based cnn architecture,” in *Proceedings of the Asian Conference on Computer Vision (ACCV)*. Springer, 2017, pp. 213–228. 1
- [7] Y. Liu *et al.*, “Application of multi-modal fusion attention mechanism in semantic segmentation,” in *Proceedings of the Asian Conference on Computer Vision (ACCV)*, 2022, pp. 1245–1264. 1
- [8] M. Cordts *et al.*, “The CityScapes dataset for semantic urban scene understanding,” in *Proceedings of the IEEE Conference on Computer Vision and Pattern Recognition (CVPR)*, 2016, pp. 3213–3223. 1, 6, 9
- [9] G. Hinton *et al.*, “Distilling the knowledge in a neural network,” *arXiv preprint arXiv:1503.02531*, 2015. 1, 2, 3, 7, 9
- [10] C. Li, G. Cheng, and J. Han, “Boosting knowledge distillation via intra-class logit distribution smoothing,” *IEEE Transactions on Circuits and Systems for Video Technology*, pp. 1–1, 2023. 1
- [11] C. Shu *et al.*, “Channel-wise knowledge distillation for dense prediction,” in *Proceedings of the IEEE/CVF International Conference on Computer Vision (ICCV)*, 2021, pp. 5311–5320. 1, 2, 3, 7, 9
- [12] S. Zagoruyko and N. Komodakis, “Paying more attention to attention: Improving the performance of convolutional neural networks via attention transfer,” *arXiv preprint arXiv:1612.03928*, 2016. 1, 2, 7, 9
- [13] J. Kim *et al.*, “Paraphrasing complex network: Network compression via factor transfer,” *Advances in Neural Information Processing Systems (NeurIPS)*, vol. 31, 2018. 1, 2, 7, 9
- [14] Z. Huang and N. Wang, “Like what you like: Knowledge distill via neuron selectivity transfer,” *arXiv preprint arXiv:1707.01219*, 2017. 1, 2, 3, 5, 7, 9
- [15] W. Park *et al.*, “Relational knowledge distillation,” in *Proceedings of the IEEE/CVF Conference on Computer Vision and Pattern Recognition (CVPR)*, 2019, pp. 3967–3976. 1, 2, 3, 5, 7, 9
- [16] F. Tung and G. Mori, “Similarity-preserving knowledge distillation,” in *Proceedings of the IEEE/CVF International Conference on Computer Vision (ICCV)*, 2019, pp. 1365–1374. 1, 2, 5, 7, 9
- [17] S. Ahn *et al.*, “Variational information distillation for knowledge transfer,” in *Proceedings of the IEEE/CVF Conference on Computer Vision and Pattern Recognition (CVPR)*, 2019, pp. 9163–9171. 1, 2, 7, 9
- [18] P. Chen *et al.*, “Distilling knowledge via knowledge review,” in *Proceedings of the IEEE/CVF Conference on Computer Vision and Pattern Recognition (CVPR)*, 2021, pp. 5008–5017. 1, 5
- [19] S. Hu *et al.*, “Multi-modal unsupervised domain adaptation for semantic image segmentation,” *Pattern Recognition*, vol. 137, p. 109299, 2023. 2
- [20] N. C. Garcia *et al.*, “Modality distillation with multiple stream networks for action recognition,” in *Proceedings of the European Conference on Computer Vision (ECCV)*, 2018, pp. 103–118. 2
- [21] C. C. Aggarwal *et al.*, *Data mining: the textbook*. Springer, 2015, vol. 1. 2, 5
- [22] B. Zhao *et al.*, “Decoupled knowledge distillation,” in *Proceedings of the IEEE/CVF Conference on Computer Vision and Pattern Recognition (CVPR)*, 2022, pp. 11953–11962. 2, 3, 4, 5, 7, 9, 10
- [23] T. Nguyen *et al.*, “Do wide and deep networks learn the same things? uncovering how neural network representations vary with width and depth,” *arXiv preprint arXiv:2010.15327*, 2020. 2, 5
- [24] W.-D. K. Ma *et al.*, “The hsic bottleneck: Deep learning without back-propagation,” in *Proceedings of the AAAI Conference on Artificial Intelligence (AAAI)*, vol. 34, no. 04, 2020, pp. 5085–5092. 2, 5

- [25] Y. Zhang *et al.*, “Deep multimodal fusion for semantic image segmentation: A survey,” *Image and Vision Computing*, vol. 105, p. 104042, 2021. [2](#)
- [26] H. Wang *et al.*, “SNE-RoadSeg+: Rethinking depth-normal translation and deep supervision for freespace detection,” in *2021 IEEE/RSJ International Conference on Intelligent Robots and Systems (IROS)*. IEEE, 2021, pp. 1140–1145. [2](#)
- [27] Q. Ha *et al.*, “MFNet: Towards real-time semantic segmentation for autonomous vehicles with multi-spectral scenes,” in *2017 IEEE/RSJ International Conference on Intelligent Robots and Systems (IROS)*. IEEE, 2017, pp. 5108–5115. [2](#)
- [28] A. Valada *et al.*, “Adapnet: Adaptive semantic segmentation in adverse environmental conditions,” in *2017 IEEE International Conference on Robotics and Automation (ICRA)*. IEEE, 2017, pp. 4644–4651. [2](#)
- [29] Y. Cheng *et al.*, “Locality-sensitive deconvolution networks with gated fusion for rgb-d indoor semantic segmentation,” in *Proceedings of the IEEE Conference on Computer Vision and Pattern Recognition (CVPR)*, 2017, pp. 3029–3037. [2](#)
- [30] X. Liu *et al.*, “Representation learning using multi-task deep neural networks for semantic classification and information retrieval,” in *Proceedings of the 2015 Conference of the North American Chapter of the Association for Computational Linguistics: Human Language Technologies*, 2015, pp. 912–921. [2](#)
- [31] A. Romero *et al.*, “FitNets: Hints for thin deep nets,” *arXiv preprint arXiv:1412.6550*, 2014. [2](#), [5](#), [7](#), [9](#)
- [32] Z. Guo *et al.*, “Boosting graph neural networks via adaptive knowledge distillation,” in *Proceedings of the AAAI Conference on Artificial Intelligence (AAAI)*, vol. 37, no. 6, 2023, pp. 7793–7801. [4](#)
- [33] B. Peng *et al.*, “Correlation congruence for knowledge distillation,” in *Proceedings of the IEEE/CVF International Conference on Computer Vision (ICCV)*, 2019, pp. 5007–5016. [5](#)
- [34] B. Heo *et al.*, “Knowledge transfer via distillation of activation boundaries formed by hidden neurons,” in *Proceedings of the AAAI Conference on Artificial Intelligence (AAAI)*, vol. 33, no. 01, 2019, pp. 3779–3787. [5](#)
- [35] J. Yim *et al.*, “A gift from knowledge distillation: Fast optimization, network minimization and transfer learning,” in *Proceedings of the IEEE Conference on Computer Vision and Pattern Recognition (CVPR)*, 2017, pp. 4133–4141. [5](#)
- [36] S. Kornblith *et al.*, “Similarity of neural network representations revisited,” in *International Conference on Machine Learning (ICML)*. PMLR, 2019, pp. 3519–3529. [5](#)
- [37] C. Cortes *et al.*, “Algorithms for learning kernels based on centered alignment,” *The Journal of Machine Learning Research*, vol. 13, no. 1, pp. 795–828, 2012. [5](#)
- [38] Y. Cabon *et al.*, “Virtual KITTI 2,” *arXiv preprint arXiv:2001.10773*, 2020. [6](#)
- [39] M. Menze and A. Geiger, “Object scene flow for autonomous vehicles,” in *Proceedings of the IEEE/CVF Conference on Computer Vision and Pattern Recognition (CVPR)*, 2015, pp. 3061–3070. [6](#)
- [40] J. Li *et al.*, “Practical stereo matching via cascaded recurrent network with adaptive correlation,” in *Proceedings of the IEEE/CVF Conference on Computer Vision and Pattern Recognition (CVPR)*, 2022, pp. 16 263–16 272. [6](#)
- [41] H. Robbins and S. Monro, “A stochastic approximation method,” *The Annals of Mathematical Statistics*, pp. 400–407, 1951. [6](#)
- [42] C. Min *et al.*, “ORFD: A dataset and benchmark for off-road freespace detection,” in *2022 International Conference on Robotics and Automation (ICRA)*. IEEE, 2022, pp. 2532–2538. [9](#)
- [43] E. Xie *et al.*, “SegFormer: Simple and efficient design for semantic segmentation with transformers,” *Advances in Neural Information Processing Systems (NeurIPS)*, vol. 34, pp. 12 077–12 090, 2021. [9](#)